frontiers | Frontiers in Molecular Biosciences

TYPE Original Research
PUBLISHED 17 May 2024
DOI 10.3389/fmolb.2024.1369000

Check for updates

OPEN ACCESS

EDITED BY
Raffaella De Pace,
National Institutes of Health (NIH), United States

REVIEWED BY
Bhavani Shankar Sahu,
National Brain Research Centre (NBRC), India
Hilda Petrs-Silva,
Federal University of Rio de Janeiro, Brazil
Rocchina Miglionico,
University of Basilicata, Italy

*CORRESPONDENCE
Blanca Arango-Gonzalez,
blanca.arango-gonzalez@klinikum.uni-tuebingen.de
Marius Ueffing,
marius.ueffing@uni-tuebingen.de

†These authors have contributed equally to this work and share senior authorship

RECEIVED 11 January 2024
ACCEPTED 23 April 2024
PUBLISHED 17 May 2024

CITATION
Cao B, Dahlen JV, Sen M, Beyer T, Leonhard T, Kilger E, Arango-Gonzalez B and Ueffing M (2024), Mutant dominant-negative *rhodopsin*$^{\Delta I256}$ causes protein aggregates degraded via ERAD and prevents normal rhodopsin from proper membrane trafficking. *Front. Mol. Biosci.* 11:1369000.
doi: 10.3389/fmolb.2024.1369000

COPYRIGHT
© 2024 Cao, Dahlen, Sen, Beyer, Leonhard, Kilger, Arango-Gonzalez and Ueffing. This is an open-access article distributed under the terms of the Creative Commons Attribution License (CC BY). The use, distribution or reproduction in other forums is permitted, provided the original author(s) and the copyright owner(s) are credited and that the original publication in this journal is cited, in accordance with accepted academic practice. No use, distribution or reproduction is permitted which does not comply with these terms.

Mutant dominant-negative *rhodopsin*$^{\Delta I256}$ causes protein aggregates degraded via ERAD and prevents normal rhodopsin from proper membrane trafficking

Bowen Cao[1,2], Johanna Valentina Dahlen[1], Merve Sen[1,2], Tina Beyer[1], Tobias Leonhard[1], Ellen Kilger[1], Blanca Arango-Gonzalez[1*†] and Marius Ueffing[1*†]

[1]Centre for Ophthalmology, Institute for Ophthalmic Research, University of Tübingen, Tuebingen, Germany, [2]Graduate Training Centre of Neuroscience, University of Tübingen, Tuebingen, Germany

Dominant mutations in the rhodopsin gene (*Rho*) contribute to 25% of autosomal dominant retinitis pigmentosa (adRP), characterized by photoreceptor loss and progressive blindness. One such mutation, *Rho*$^{\Delta I256}$, carries a 3-bp deletion, resulting in the loss of one of two isoleucines at codons 255 and 256. Our investigation, using recombinant expression in HEK293 and COS-7 cells, revealed that *Rho*$^{\Delta I256}$, akin to the known adRP mutation *Rho*^{P23H}, induces the formation of rhodopsin protein (RHO) aggregates at the perinuclear region. Co-expression of *Rho*$^{\Delta I256}$ or *Rho*^{P23H} with wild-type *Rho*^{WT}, mimicking the heterozygous genotype of adRP patients, demonstrated the dominant-negative effect, as all isoforms were retained in perinuclear aggregates, impeding membrane trafficking. In retinal explants from WT mice, mislocalization of labeled adRP isoforms at the outer nuclear layer was observed. Further analysis revealed that RHO$^{\Delta I256}$ aggregates are retained at the endoplasmic reticulum (ER), undergo ER-associated degradation (ERAD), and colocalize with the AAA-ATPase escort chaperone valosin-containing protein (VCP). These aggregates are polyubiquitinated and partially colocalized with the 20S proteasome subunit beta-5 (PSMB5). Pharmacological inhibition of proteasome- or VCP activity increased RHO$^{\Delta I256}$ aggregate size. In summary, RHO$^{\Delta I256}$ exhibits dominant pathogenicity by sequestering normal RHO^{WT} in ER aggregates, preventing its membrane trafficking and following the ERAD degradation.

KEYWORDS

rhodopsin, ADRP, dominant-negative effect, VCP, ERAD, proteasome, retinitis pigmentosa

1 Introduction

Retinitis pigmentosa (RP) is a progressive rod-cone dystrophy caused by the dysfunction and eventual death of rod photoreceptors, followed by cone photoreceptor cell death. Initial symptoms of this disease include impaired dark adaptation and "night blindness" (nyctalopia), followed by a loss of peripheral vision and, in advanced cases,

possible tunnel vision. As the disease progresses, central vision is also affected (Hartong et al., 2006). RP is currently incurable and is the leading cause of visual impairment and blindness in individuals under the age of 60 (Cross et al., 2022). While clinical therapy cannot reverse the damage caused by RP, efforts are focused on slowing down visual deterioration, treating complications, and helping patients cope with the psychosocial impact of their condition (Frick et al., 2012).

The rhodopsin gene (*Rho*) was the first gene identified to cause RP. This gene encodes Rhodopsin protein (RHO), a seven-transmembrane G-protein-coupled receptor expressed exclusively in mammalian rod photoreceptors. RHO is synthesized and folded in the endoplasmic reticulum (ER) and processed in the Golgi (Deretic, 2006). Proper folding and trafficking of RHO is essential for normal phototransduction and rod cell survival. The fully functional form of RHO consists of the apoprotein opsin, which binds the chromophore 11-cis retinal (Hargrave, 2001; Pearring et al., 2013). RHO accounts for approximately 90% of all proteins in the discs. Its absence prevents outer segment (OS) formation and leads to photoreceptor cell death (Berson, 1996; Humphries et al., 1997; Lem et al., 1999; Rakshit and Park, 2015).

Rho-mediated RP can be inherited in an autosomal dominant (adRP) or autosomal recessive (arRP) pattern. In the adRP cases, over 150 mutations in the *Rho* gene have been identified, accounting for 20%–30% of all adRP cases (Athanasiou et al., 2018). Researchers have attempted to categorize these mutations based on their biochemical and cellular properties (Inglehearn et al., 1991; Kaushal and Khorana, 1994; Mendes et al., 2005; Krebs et al., 2010; Rakoczy et al., 2011). Interestingly, most Rho mutations fall into class II, characterized by protein misfolding, ER retention, and OS instability (Athanasiou et al., 2018).

A 3-base pair (bp) deletion in the human *Rho* gene, deleting one of the two isoleucine (I) at codon 255 or 256 in the sixth transmembrane domain (referred to in this paper as $Rho^{\Delta I256}$), has been suggested to be the major cause of adRP in Europe (Inglehearn et al., 1991; Artlich et al., 1992). $Rho^{\Delta I256}$ was first discovered in a British family (Inglehearn et al., 1991) and later found in German, Belgian, and Chinese families (Lorenz et al., 1993a; Li et al., 2010). Patients with this mutation show clinical symptoms and signs of RP with an early onset of nyctalopia, a constricted visual field, and even reduced visual acuity or color vision abnormalities (Lorenz et al., 1993a; Li et al., 2010). However, the biochemical changes or associated molecular mechanisms that link the $Rho^{\Delta I256}$ mutation to photoreceptor cell death are still not fully understood. According to Sung *et al.*, $Rho^{\Delta I256}$ causes biochemical defects associated with class II mutations, with $RHO^{\Delta I256}$ protein localizing and accumulating in the ER (Sung et al., 1993). However, the mechanisms underlying how this mutation leads to photoreceptor cell death remain unclear.

It has been reported that cells with dominant *Rho* mutations undergo cell death as a result of toxic gain-of-function (GOF) and/or dominant-negative (DN) activity (Athanasiou et al., 2018). GOF mechanisms include protein misfolding, aggregation formation, and unfolded protein response (UPR) induction. On the other hand, DN effects of dominant *Rho* mutations may eliminate one or more functions associated with normal RHO, affecting the maturation, trafficking, and activity of wild-type RHO (RHO^{WT}). RP caused by the DN mechanisms may be due to RHO aggregates that interfere with endogenous RHO maturation (Wilson and Wensel, 2003). These two mechanisms are supported by studies of the Rho^{P23H} (proline to histidine substitution at position 23) class II mutation (Illing et al., 2002; Saliba PMM et al., 2002; Rajan and Kopito, 2005; Griciuc, 2010). Rho^{P23H} is the most common *Rho* mutation in North America and arguably the most studied one, accounting for 10% of all cases of adRP in the US in patients of Western European origin (Sullivan et al., 2006). The Rho^{P23H} mutant forms ER-bound aggregates and interferes with the UPR system. In addition, these aggregates prevent the proper processing of RHO^{WT}.

According to several studies, $Rho^{\Delta I256}$ and Rho^{P23H} exhibit similar phenotypes (Dryja et al., 1990; Lorenz et al., 1993b; Naash et al., 1993; Sung et al., 1993; Kaushal and Khorana, 1994; Daiger et al., 2007), probably because mutations affecting *Rho* transmembrane or intradiscal domain residues are generally classified as class II mutations (Lorenz et al., 1993b), suggesting that $Rho^{\Delta I256}$ may share a similar pathogenetic mechanism with Rho^{P23H}. In previous studies, we could show that RHO^{P23H} aggregate formation is coupled to ER-associated protein degradation (ERAD) (Griciuc et al., 2010a), a major protein processing pathway that is divided into four steps: substrate recognition, ubiquitination, retrotranslocation to the cytosol, and proteasome-mediated degradation (Guerriero and Brodsky, 2012). Further, we found that misfolded RHO^{P23H} is targeted by valosin-containing protein (VCP), a type II AAA ATPase chaperone that processes and earmarks RHO^{P23H} to be transferred from the endoplasmic reticulum (ER) to the proteasome system for degradation (Wang et al., 2004). VCP is the driving force for the retrotranslocation of ER-retained aggregates from the ER to the cytosol for proteasomal degradation (Ye et al., 2001). Studies have shown that VCP interacts with aggregates or ubiquitin-positive inclusions in patients with neurodegenerative diseases (Mizuno et al., 2003; Boeddrich et al., 2006; Gitcho et al., 2009). Our previous research has also shown that inhibition of VCP activity suppresses retinal pathology and preserves retinal structure and function in Rho^{P23H}-associated adRP animal models (Griciuc et al., 2010b; Arango-Gonzalez et al., 2020; Sen et al., 2021a; Sen et al., 2021b). Here, we show that, similar to Rho^{P23H}, degradation of $RHO^{\Delta I256}$ aggregates undergoes a VCP-dependent ERAD process. Most importantly, we find that $RHO^{\Delta I256}$-containing cytoplasmic aggregates retain RHO^{WT} and interfere with the normal localization or trafficking of RHO^{WT} to the cell membrane, which explains its dominant-negative mechanism. (All abbreviations are shown in Supplementary Table S1).

2 Results

2.1 $Rho^{\Delta I256}$ mutant is mislocalized and tends to form high molecular weight aggregates in the cytosol

To study the cellular behavior of $Rho^{\Delta I256}$ *in vitro*, we transfected different *Rho* constructs (Rho^{WT}, Rho^{P23H}, or $Rho^{\Delta I256}$), tagged with EGFP using the pEGFP-N1 vector, into HEK293 and COS-7 cells (Figure 1). As expected, RHO^{WT}-EGFP was correctly targeted and evenly distributed to the plasma membrane in both cell types, with only scattered RHO^{WT}-EGFP puncta in the cytosol, which is

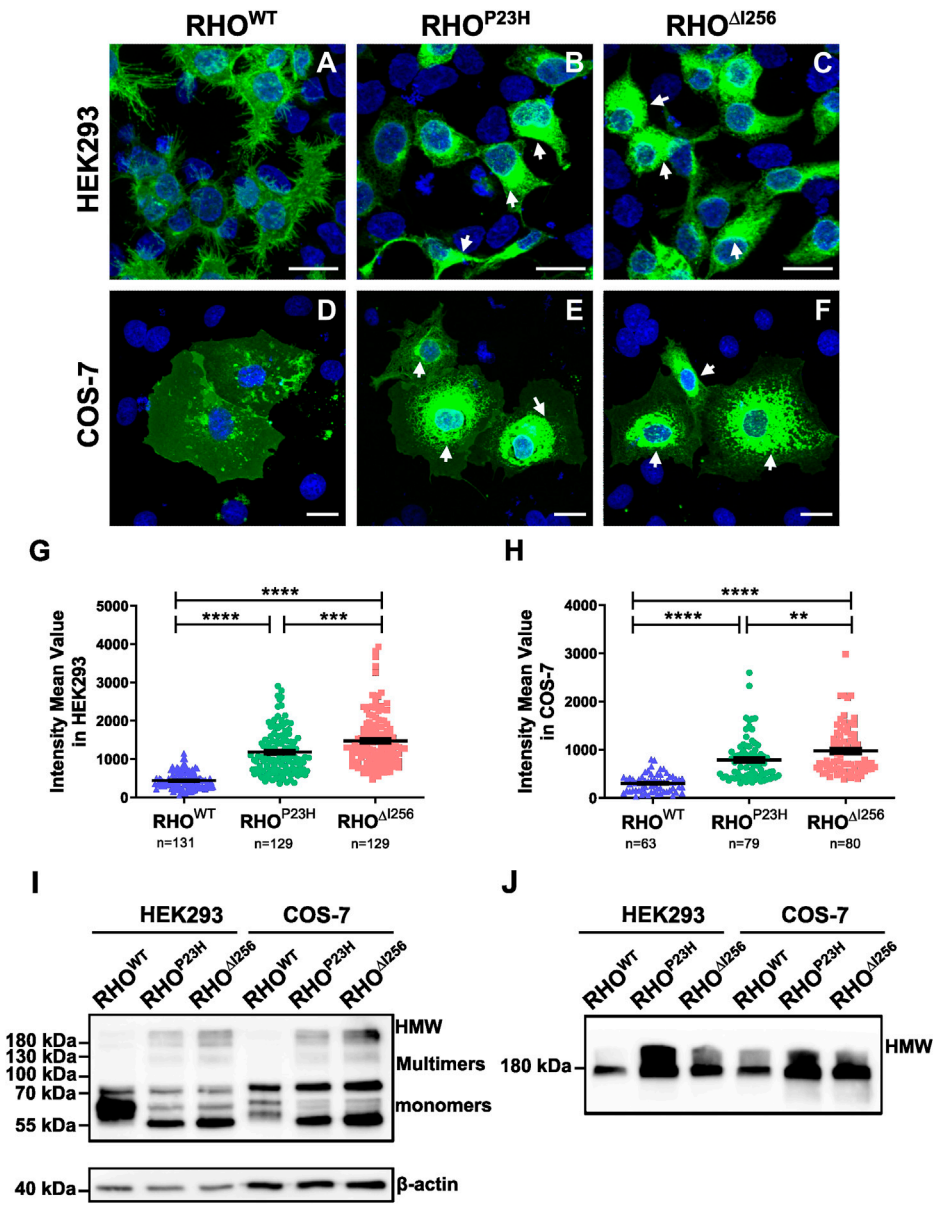

FIGURE 1
RHO$^{\Delta I256}$ mislocalizes to the cytosol and forms high molecular weight aggregates *in vitro*. Fluorescence images of HEK293 **(A–C)** and COS-7 cells **(D–F)** transfected with *Rho*^{WT}-EGFP, *Rho*^{P23H}-EGFP, or *Rho*$^{\Delta I256}$-EGFP (green). RHO^{WT}-EGFP is predominantly localized at the plasma membrane, while RHO$^{\Delta I256}$-EGFP (white arrows in C, F) and RHO^{P23H}-EGFP (white arrows in B, E) accumulate in the cytosol. Scale bar: 20 μm. There was a significant increase in the mean fluorescence intensity (MFI) in cells transfected with *Rho*$^{\Delta I256}$-EGFP or *Rho*^{P23H}-EGFP cells compared to *Rho*^{WT}-EGFP **(G–H)**. Immunoblot analysis revealed that RHO$^{\Delta I256}$-EGFP forms HMW aggregates in both soluble **(I)** and insoluble cell fractions **(J)**. Data were expressed as mean ± SEM. Significance was calculated by Mann-Whitney-U-test. $^{**}p < 0.01$, $^{***}p < 0.001$, $^{****}p < 0.0001$.

consistent with previous results (Figure 1A, D) (Illing et al., 2002; Saliba PMM et al., 2002; Griciuc et al., 2010a). In contrast, most RHO$^{\Delta I256}$ was confined to the perinuclear region, with high fluorescence intensity (Figure 1C, F), similar to the cellular localization of RHO^{P23H} (Figure 1B, E). We measured the mean fluorescence intensity (MFI) in the cytoplasmic region for all three groups to quantify RHO aggregation. We found that the MFI of RHO was significantly increased in both *Rho*$^{\Delta I256}$-EGFP and *Rho*^{P23H}-EGFP transfected cells (HEK293 cells: 1,477 ± 695.9; COS-7 cells: 974.2 ± 503.3; HEK293 cells: 1,182 ± 570.9; COS-7 cells: 788.1 ± 445.8, respectively) compared to *Rho*^{WT}-EGFP transfected cells (HEK293 cells: 438.8 ± 207.9; COS-7 cells: 303.2 ± 181.6) (Figures 1G, H), indicating that *Rho*$^{\Delta I256}$, similar to *Rho*^{P23H}, leads to a high degree of RHO accumulation. We also found that *Rho*$^{\Delta I256}$-EGFP results in a significantly higher MFI than *Rho*^{P23H}-EGFP (HEK293 cells: *Rho*$^{\Delta I256}$ vs. *Rho*^{P23H} $p < 0.0001$; COS-7 cells: *Rho*$^{\Delta I256}$ vs. *Rho*^{P23H} $p < 0.05$, Mann-Whitney-U-test, at least 40 cells in HEK293 and 20 cells in COS-7 cells from three different experiment were quantified), suggesting that the *Rho*$^{\Delta I256}$ mutation induces more severe protein aggregation.

Given the potential influence of large EGFP tags on the structure, oligomerization, and aggregate formation of the target

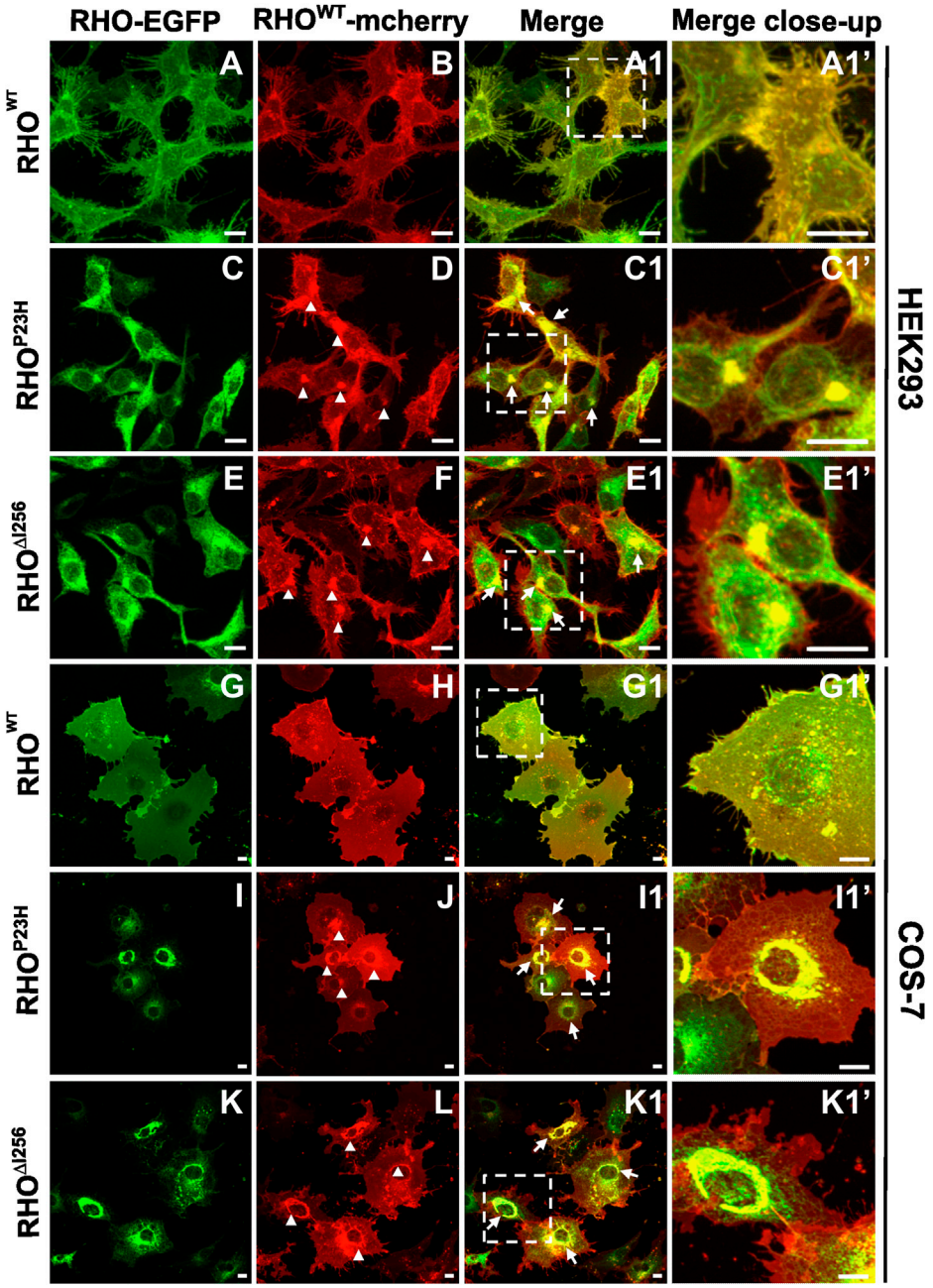

FIGURE 2
Rho$^{\Delta I256}$-EGFP and *Rho*^{WT}-mcherry co-expression causes intracellular retention of WT rhodopsin. Fluorescence microscopy detecting EGFP **(A, C, E, G, I, K)** and mcherry **(B, D, F, H, J, L)** in HEK293 and COS-7 cells co-transfected with *Rho*^{WT}-mcherry and *Rho*$^{\Delta I256}$-EGFP or *Rho*^{P23H}-EGFP plasmids. **(A1, C1, E1, G1, I1, and K1)** show the merged images of the EGFP and mcherry channels. Arrows indicate the colocalization of RHO^{WT}-mcherry with RHO$^{\Delta I256}$-EGFP or RHO^{P23H}-EGFP. Magnified view is shown in **(A1′, C1′, E1′, G1′, I1′, and K1′)**. Arrowheads mark the mislocalized RHO^{WT} retained in misfolded aggregates **(D, F, J, L)**. Scale bar: 10 μm.

protein, we transfected HEK293 cells with pEGFP-N1 plasmids encoding only EGFP. We compared the behavior of this control group with that of cells transfected with *Rho*^{WT}-EGFP, *Rho*^{P23H}-EGFP, or *Rho*$^{\Delta I256}$-EGFP. Remarkably, cells transfected with the plasmid encoding only EGFP did not exhibit aggregate formation (Supplementary Figure S1), a finding consistent with previous studies (Griciuc et al., 2010a). To further investigate the component of the accumulated RHO aggregates in the cytoplasm, we monitored RHO levels in detergent-soluble (Figure 1I) and detergent-insoluble (Figure 1J) extracts from HEK293 cells that had been transiently transfected with *Rho*^{WT}-EGFP, *Rho*$^{\Delta I256}$-EGFP, or *Rho*^{P23H}-EGFP constructs using SDS-PAGE Western blotting. The mature monomeric form of RHO containing the EGFP tag was observed as a band at 55–75 kDa, whereas dimers and trimers appear as smears at approximately 130 kDa and 180 kDa, respectively. High molecular weight (HMW) species with molecular weights greater than 180 kDa indicated RHO-containing oligomers and aggregates. RHO^{WT}-EGFP was mostly

detected in soluble extracts (Figure 1I) and showed diffuse bands of the predominantly monomeric form of the mature RHO, with minor multimers or HMW RHO. These results suggest that most RHO^{WT}-EGFP forms a native mature conformation (Griciuc et al., 2010a).

On the other hand, $RHO^{\Delta I256}$-EGFP showed a completely different behavior. Most of the mutant RHO was found in dimers, trimers, and HMW oligomers in the soluble cell fraction (Figure 1I), indicating a non-native conformation or immature RHO since RHO is monomeric in its native form in the membrane (Downer and Cone, 1985). Furthermore, a significant amount of $RHO^{\Delta I256}$-EGFP appeared as HMW species in the detergent-insoluble fractions (Figure 1J) compared to RHO^{WT}-EGFP, suggesting that *Rho*$^{\Delta I256}$ is more likely to form RHO aggregates than RHO^{WT}. Similar observations were also made for RHO^{P23H}-EGFP.

In conclusion, our results suggest that *Rho*$^{\Delta I256}$, like the *Rho*^{P23H} mutation, causes a mislocalization of RHO that cannot be effectively targeted to the plasma membrane. In addition, mutant RHO is more prone to form cytosolic non-native HMW aggregates than RHO^{WT}.

2.2 Dominant *Rho*$^{\Delta I256}$ mutation impairs the localization of WT rhodopsin

Most, if not all, patients with adRP carrying the *Rho*$^{\Delta I256}$ mutation inherit one mutant allele and one normal (WT) allele (Inglehearn et al., 1991; Lorenz et al., 1993a; Li et al., 2010). To closely mimic the heterozygous nature of the human patient genotype, we co-transfected HEK293 and COS-7 cells with EGFP-tagged *Rho*$^{\Delta I256}$, *Rho*^{P23H}, or *Rho*^{WT} and mcherry-tagged *Rho*^{WT} at equal concentrations. We used the two fluorescent tags to visualize any colocalization or interaction between mutant $RHO^{\Delta I256}$ and RHO^{WT}.

Co-transfection of *Rho*$^{\Delta I256}$-EGFP and *Rho*^{WT}-mcherry in HEK293 and COS-7 cells resulted in intracellular mislocalization of $RHO^{\Delta I256}$-EGFP as previously observed (Figure 2E, K). Here, RHO^{WT}-mcherry was also mislocalized to the perinuclear region and overlapped significantly with $Rho^{\Delta I256}$-EGFP aggregates (Figure 2E1, K1). In comparison, when co-expressing both differently tagged *Rho*^{WT} plasmids, RHO^{WT}-EGFP and RHO^{WT}-mcherry were predominantly localized to the plasma membrane (Figure 2A, B, G, H), as previously observed for RHO^{WT}. These results indicate that $RHO^{\Delta I256}$ impairs the correct membrane localization of the RHO^{WT} protein. Since a fraction of RHO^{WT}-mcherry was still targeted to the cell membrane in cells co-transfected with mutant RHO, this suggests that the impairment of RHO^{WT} was not complete. Similar results were obtained in cells co-expressing RHO^{WT}-mcherry with RHO^{P23H}-EGFP (Figures 2I,J), indicating that the molecular pathomechanisms underlying the two dominant *Rho* mutations are likely similar.

Our results show that mislocalized $RHO^{\Delta I256}$ aggregates trap part of RHO^{WT} in the aggregate pool, preventing RHO^{WT} from reaching its correct location in the cell membrane. As a result, a dominant-negative (DN) effect may play an important role in the pathology of *Rho*$^{\Delta I256}$-associated retinal degeneration (Herskowitz, 1987).

2.3 Proper targeting of endogenous WT rhodopsin to the photoreceptor outer segment is compromised by exogenously expressed $RHO^{\Delta I256}$ in C57BL/6J retinal explants

The recruitment of RHO^{WT} into the $RHO^{\Delta I256}$ aggregates in cells supports the hypothesis that the *Rho*$^{\Delta I256}$ allele causes RP via a DN mechanism. To investigate this, we transfected *Rho*$^{\Delta I256}$-EGFP into retinal explants from C57BL/6J (wild-type, WT) mice, which naturally produce RHO^{WT} that localizes to the rod outer segments (ROS). To determine whether $RHO^{\Delta I256}$ affects endogenous RHO^{WT} localization, we used reverse magnetofection, a technique to deliver *Rho*$^{\Delta I256}$-EGFP into the C57BL/6J retina (Gomez-Tourino et al., 2013; Sen et al., 2021a; Bassetto et al., 2021). We labeled total RHO with a specific red fluorescing dye conjugated antibody to differentiate between EGFP-tagged exogenous RHO (displayed fluorescence in both red and green) and endogenous RHO (exhibited only red fluorescence). The comprehensive details on the *Rho*$^{\Delta I256}$-EGFP transfection group as well as other transfection groups, are listed in Supplementary Table S2.

When C57BL/6J retinal explants were transfected with *the* *Rho*^{WT}-EGFP/XPMag complex, both endogenous and exogenous RHO^{WT} correctly targeted the OS layer and largely overlapped each other. However, when the C57BL/6J retinal explants were transfected with the *Rho*$^{\Delta I256}$-EGFP/XPMag complex, a significant amount of endogenous RHO^{WT} was mislocalized and remained in the ONL instead of being properly targeted to the OS (Figure 3). As expected, exogenous $RHO^{\Delta I256}$-EGFP was trapped in the ONL and overlapped with part of endogenous RHO^{WT}. We observed the same result in the *Rho*^{P23H}-EGFP/XPMag-transfected C57BL/6J retinal explants. Furthermore, transfection of either of these two dominant *Rho* mutants into C57BL/6J retinal explants resulted in reduced OS length (Figure 3), which is a hallmark of retinal degeneration, indicating a degenerative effect (Milam et al., 1996; Sakai et al., 2003). Endogenous RHO was correctly targeted to the OS in all three control groups (complete medium CM, XPMag, or EGFP-transfected groups, as shown in Supplementary Figure S2).

Our findings support the hypothesis that the transport of endogenous RHO^{WT} is impaired in the presence of the dominant *Rho*$^{\Delta I256}$ (or *Rho*^{P23H}) mutant, suggesting that the DN effect plays an essential role in the pathophysiology of *Rho*$^{\Delta I256}$-associated adRP.

2.4 $RHO^{\Delta I256}$ is retained at the ER and forms a complex with the ERAD effector VCP

Our results show that the dominant *Rho*$^{\Delta I256}$ mutation leads to cytoplasmic aggregates retaining WT rhodopsin from reaching its final physiological destination at the membrane. We and others have previously shown that such aggregates can be substrate to ERAD, the major degradation pathway for unfolded or misfolded protein aggregates. To determine whether $RHO^{\Delta I256}$ aggregates are substrates of the ERAD clearance pathway, we analyzed whether they are tethered to ER sites and recognized by the ERAD effector VCP (Griciuc et al., 2010a; Sen et al., 2021b).

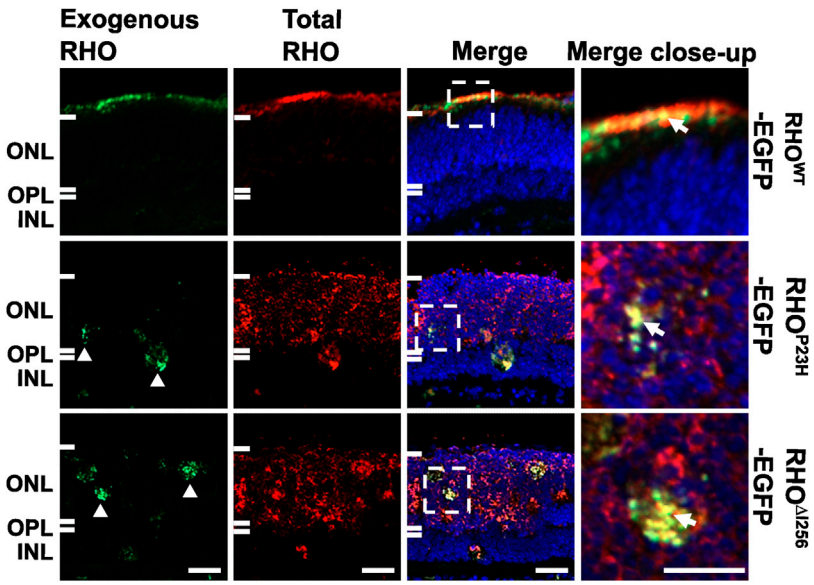

FIGURE 3
In C57BL/6J retinal explants, the trafficking of endogenous RHO^{WT} is affected by transfection with *Rho*$^{\Delta I256}$. Immunofluorescence pictures reveal the localization of total RHO (red, second column), including endogenously expressed RHO and EGFP-tagged exogenously expressed RHO in three experimental groups in C57BL/6J retinae transfected with *Rho*^{WT}-EGFP/XPMag (first row), *Rho*^{P23H}-EGFP/XPMag (second row), and *Rho*$^{\Delta I256}$-EGFP/XPMag (third row). Exogenously expressed RHO (green, first column) is indicated by EGFP fluorescence. Exogenous RHO$^{\Delta I256}$-EGFP is mislocalized in the ONL (white arrowheads, green channel) and leads to the mislocalization of endogenous RHO^{WT} (red, third row). Moreover, in *Rho*$^{\Delta I256}$-EGFP/XPMag transfected C57BL/6J mouse retinal explants, mislocalized RHO$^{\Delta I256}$-EGFP partially overlaps endogenous RHO^{WT} (white arrows, merged close-up), and the OS layer is thinner. In contrast, exogenous RHO^{WT}-EGFP correctly targets the OS layer and colocalizes with endogenously expressed RHO^{WT} in transfected C57BL/6J mouse retinal explants. Scale bar: 20 μm.

We transfected HEK293 or COS-7 cells with plasmids encoding EGFP-tagged *Rho*$^{\Delta I256}$, *Rho*^{P23H}, or *Rho*^{WT} and analyzed colocalization of RHO-EGFP with ER or VCP by immunofluorescence staining with calnexin- or VCP-specific antibodies. Our results revealed a partial colocalization between RHO$^{\Delta I256}$ aggregates with ER and VCP in both cell lines (Figure 4). In *Rho*^{WT}-EGFP transfected cells, we hardly observed any colocalization of RHO^{WT} with calnexin or VCP (Figure 4A1', J1'). In contrast, in *Rho*$^{\Delta I256}$-EGFP transfected cells, aggregated mutant RHO$^{\Delta I256}$ partially colocalized with the ER marker calnexin and with VCP (Figure 4G1, P1 and black arrows in G1', P1'). Furthermore, some of the RHO$^{\Delta I256}$-containing cytoplasmic aggregates were not found within the ER but only co-stained with VCP, indicating that they were extracted from the ER and delivered to the cytosol by VCP. Similarly, the *Rho*^{P23H} mutation led to the formation of aggregates that colocalized with calnexin and VCP, in agreement with our previous results (Griciuc et al., 2010a). Using Pearson's correlation coefficient analysis, we further quantified the colocalization between RHO and ER or VCP (Supplementary Figure S3A, B). Compared with RHO^{WT} protein, RHO$^{\Delta I256}$ and RHO^{P23H} aggregates showed significantly increased association with ER or VCP, which was consistent with the above immunostaining data.

The localization of endogenous VCP was observed predominantly in the cytoplasm in *Rho*^{WT}-EGFP-transfected cells (Figure 4C, L). However, in cells that express mutant RHO$^{\Delta I256}$ (Figure 4I, R) or RHO^{P23H} (Figure 4F, O), the distribution of VCP mostly colocalized with calnexin, suggesting that the recruitment of VCP to the ER is involved in the retrotranslocation of aggregates.

2.5 Mislocalized RHO$^{\Delta I256}$ aggregates are partially polyubiquitinated

It is known that almost all ERAD substrates are ubiquitinated prior to targeting the proteasome (Illing et al., 2002). In order to evaluate the role of ubiquitin (Ub) in the degradation of RHO$^{\Delta I256}$ aggregates or RHO^{WT}, we compared the changes in the localization and expression levels of ubiquitin proteins in *Rho*$^{\Delta I256}$-EGFP or *Rho*^{WT}-EGFP transfected cells using ubiquitin-specific antibodies. *Rho*^{P23H}-EGFP transfected cells were used as a positive control since RHO^{P23H} is much more ubiquitinated than RHO^{WT} (Illing et al., 2002).

We found that RHO$^{\Delta I256}$ aggregates were strongly ubiquitinated in transfected HEK293 and COS-7 cells colocalizing with endogenous ubiquitin (Figure 5). In both cell types transfected with *Rho*^{WT}-EGFP, ubiquitin was not specifically colocalized with rhodopsin, yet distributed throughout the whole cytosol (Figure 5B, H). No enhanced colocalization between RHO^{WT} and ubiquitin was observed in merged images (Figure 5A1, G1). In contrast, in *Rho*$^{\Delta I256}$-EGFP transfected HEK293 cells, ubiquitin staining was found in numerous accumulated puncta (Figure 5F), which localized with RHO aggregates in the cytosol (Figure 5E1', C1'). In COS-7 cells, the ubiquitin staining pattern was less punctated, more clustered (Figure 5L), and was mainly recruited to the RHO

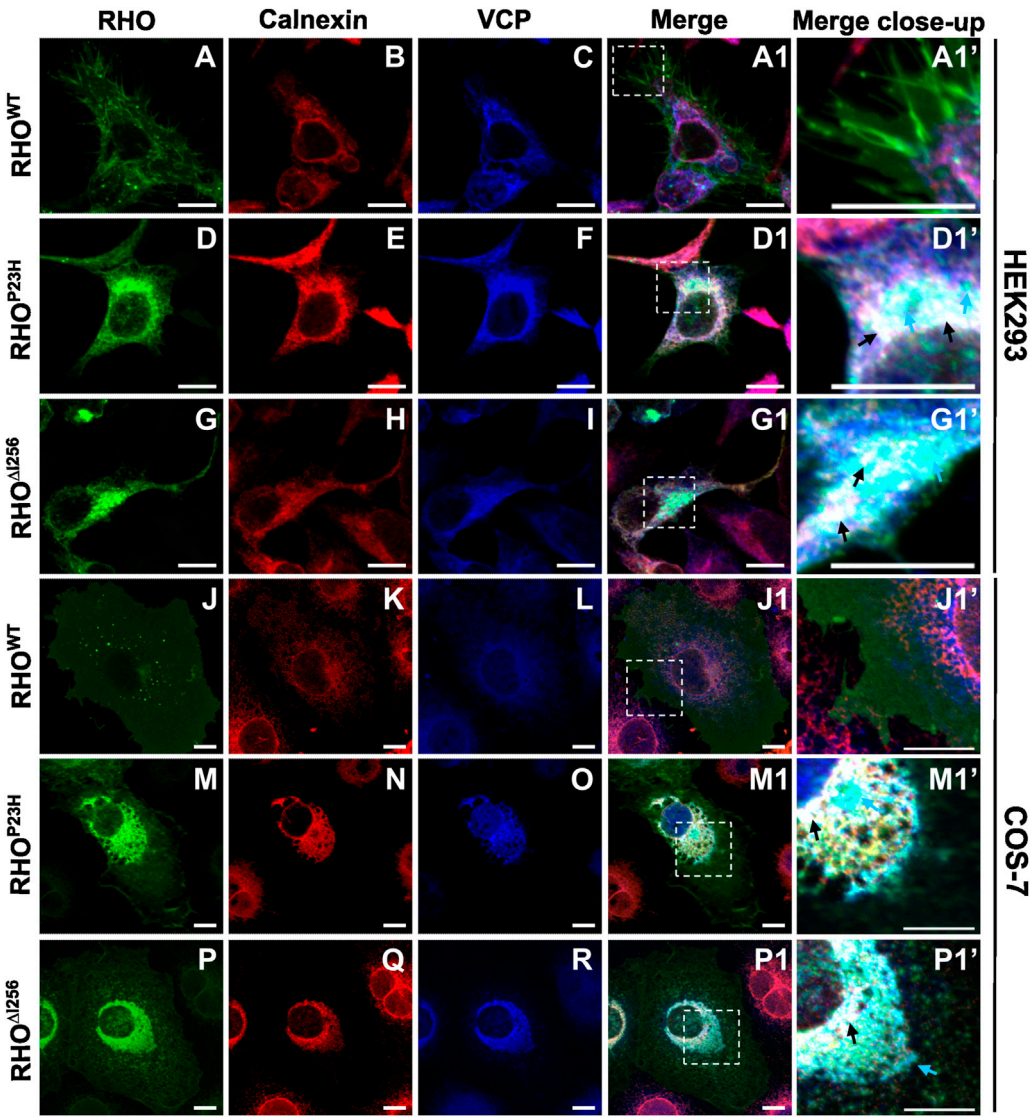

FIGURE 4
RHO$^{\Delta I256}$ aggregates colocalize with ER and VCP. Immunofluorescence staining shows the localization of transfected *Rho*-EGFP (green, first column), the ER marker Calnexin (red, second column), and endogenous VCP (blue, third column) in HEK293 **(A–I, A1, D1, G1)** or COS-7 cells **(J–R, J1, M1, P1)**. Colocalization is revealed in merged pictures (fourth column), and higher magnification pictures from merged insets are shown in column 5. RHO^{WT} is mainly localized to the plasma membrane (A and J). RHO$^{\Delta I256}$ aggregates localize with VCP to the ER (black arrows, **D1', M1'**) and partially colocalize only with VCP (cyan arrows, **D1', M1'**). RHO^{P23H} also accumulates in ER and VCP (black arrows, **G1', P1'**). Scale bar: 10 μm.

aggregates pool (Figure 5K1', I1'). A similar ubiquitin pattern to that in *Rho*$^{\Delta I256}$-EGFP transfected was seen in *Rho*^{P23H}-EGFP transfected cells. Consistent with these immunostaining results, Pearson's correlation coefficient analysis also revealed a significantly higher colocalization between RHO$^{\Delta I256}$ (or RHO^{P23H}) aggregates and Ub in contrast to RHO^{WT} (Supplementary Figure S3C).

Subsequently, we used immunoblotting to examine the expression pattern of ubiquitin in lysates of untransfected HEK293 cells and in cells transfected with different *Rho* constructs (untransfected cells were used as control) and demonstrated that similar to RHO^{P23H}, RHO$^{\Delta I256}$ is ubiquitinated to a greater extent than RHO^{WT}. We detected a significantly increased intensity of the characteristic ubiquitin smear bands in lysates obtained from mutant *Rho*$^{\Delta I256}$ or *Rho*^{P23H} transfected cells compared to those obtained from *Rho*^{WT} transfected cells (Figure 5M), particularly evident in polyubiquitin chains larger than 180 kDa. The untransfected control cells also showed the same pattern of Ub expression, indicating that the ubiquitin signal is not due to overexpression. To quantify the expression of polyubiquitin protein, we compared the levels between WT transfected group and the mutant transfected groups (protein level higher than 20 kDa). The results showed that polyubiquitin was significantly increased in HEK293 cells expressing RHO$^{\Delta I256}$ and RHO^{P23H} than in RHO^{WT} (Figure 5N). As ubiquitin acts as a tag that identifies proteins for ERAD-mediated degradation, our results indicate that ubiquitinated RHO$^{\Delta I256}$ aggregates are likely to be a substrate of the ERAD pathway.

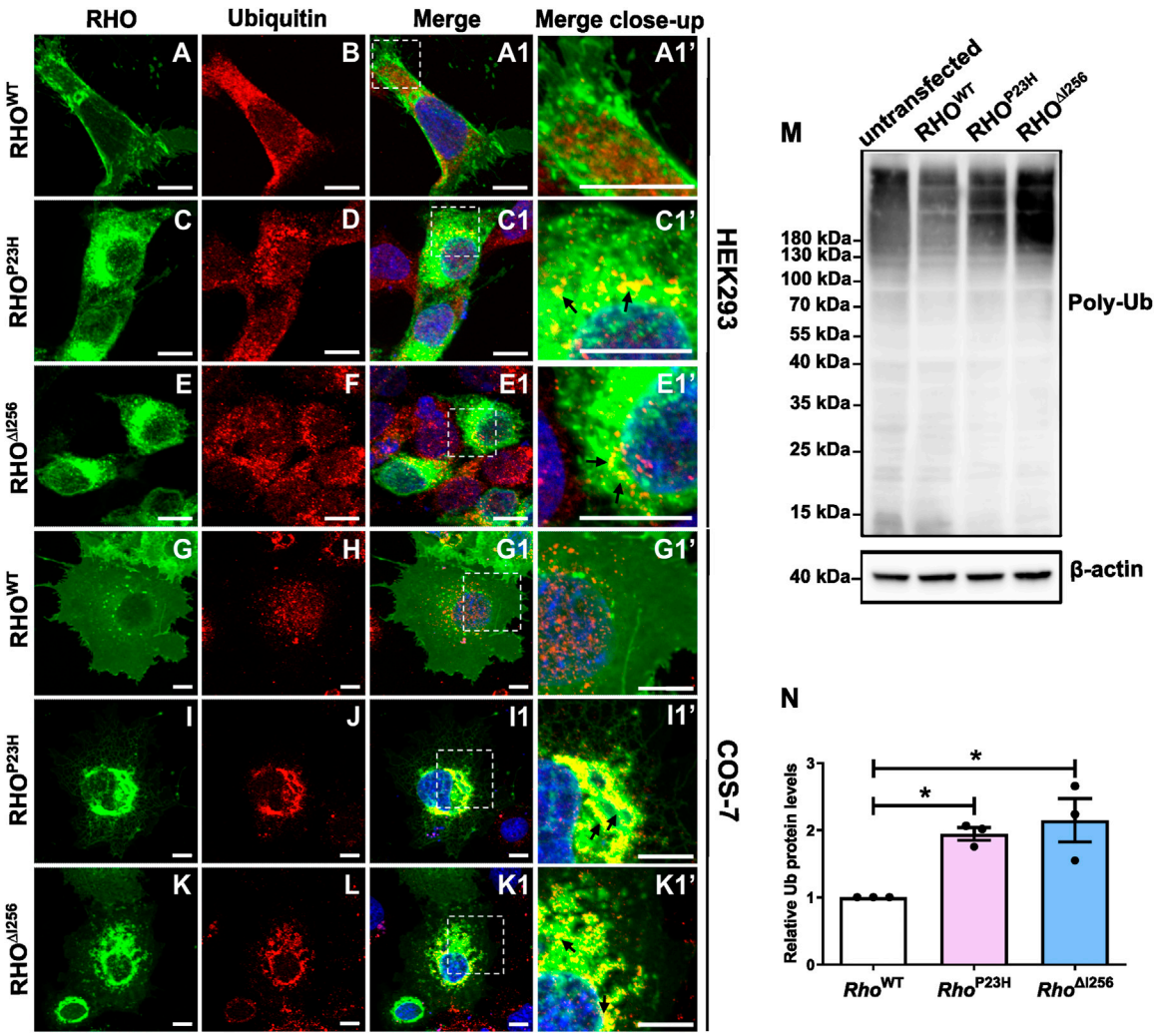

FIGURE 5
Misfolded RHO$^{\Delta I256}$ is ubiquitinated. **(A–L)** Immunofluorescence of EGFP-tagged RHO^{WT}, RHO$^{\Delta I256}$, or RHO^{P23H} (green, first column) and Ub (red, second column) in HEK293 **(A–F, A1, A1′-E1, E1′)** and COS-7 cells **(G–L, G1, G1′-K1, K1′)**. Colocalization is shown in merged pictures (third column). Ub is recruited into the aggregates pool, which is revealed as yellow dots in merged pictures in *Rho*$^{\Delta I256}$ (black arrows, **E1′, K1′**) or *Rho*^{P23H} transfected cells (black arrows, **C1′, I1′**). Scale bar: 10 μm; **(M)**. Western blot results show enhanced smear Ub bands in cell lysates of *Rho*$^{\Delta I256}$ or *Rho*^{P23H} compared to *Rho*^{WT}-transfected HEK293 cells. Ub expression is also present in untransfected control group. β-actin is used as housekeeping marker. **(N)**. Quantification of Ub expression. Data are expressed as mean ± SEM. Statistical significance was determined by one-way ANOVA followed by Bonferroni's multiple comparison test (*$p < 0.05$). Three independent experiments were included in the data analysis.

2.6 RHO$^{\Delta I256}$ colocalizes with the proteasome 20S subunit

The process of ERAD culminates with the degradation of misfolded proteins by the ubiquitin-proteasome system (UPS). In this process, substrates are tagged with ubiquitin (Ub), form polyubiquitinated adducts, and are then recognized and degraded by the 26S proteasome (Bence et al., 2001; Adams, 2003; Schwartz and Ciechanover, 2009; Sen et al., 2021b). The 26S proteasome consists of one 20S protein subunit and two 19S regulatory cap subunits. The 20S core region is responsible for substrate degradation (Gomez-Tourino et al., 2013). To analyze proteasomal rhodopsin degradation, we used a specific antibody against the proteasome 20S subunit beta 5 (PSMB5) to visualize this subunit in HEK293 and COS-7 cells transfected with plasmids encoding *Rho* and to observe its colocalization with RHO$^{\Delta I256}$ aggregates.

We found that RHO$^{\Delta I256}$ aggregates were transported to the proteasome system and colocalized with PSMB5. In *Rho*^{WT}-EGFP-transfected HEK293 and COS-7 cells, PSMB5 staining was shown in the cytoplasm and the nucleus (Figure 6B, H). However, in RHO$^{\Delta I256}$-EGFP-expressing cells, PSMB5 accumulated and formed perinuclear punctate aggregates in the cytosol. This phenomenon was more pronounced in COS-7 cells than in HEK293 cells (Figure 6D, F, J, L). Most importantly, the punctate distribution of PSMB5 overlapped with a fraction of perinuclear RHO$^{\Delta I256}$ aggregates (Figure 6C1′, I1′, J1′, K1′). Pearson's correlation coefficient analysis also showed a significantly greater colocalization between RHO$^{\Delta I256}$ (or RHO^{P23H}) aggregates and PSMB5 than RHO^{WT} (Supplementary Figure S3D). These results suggest that a fraction of these aggregates have already been retrotranslocated from the ER to the proteasome system, probably as a consequence of ERAD-mediated degradation.

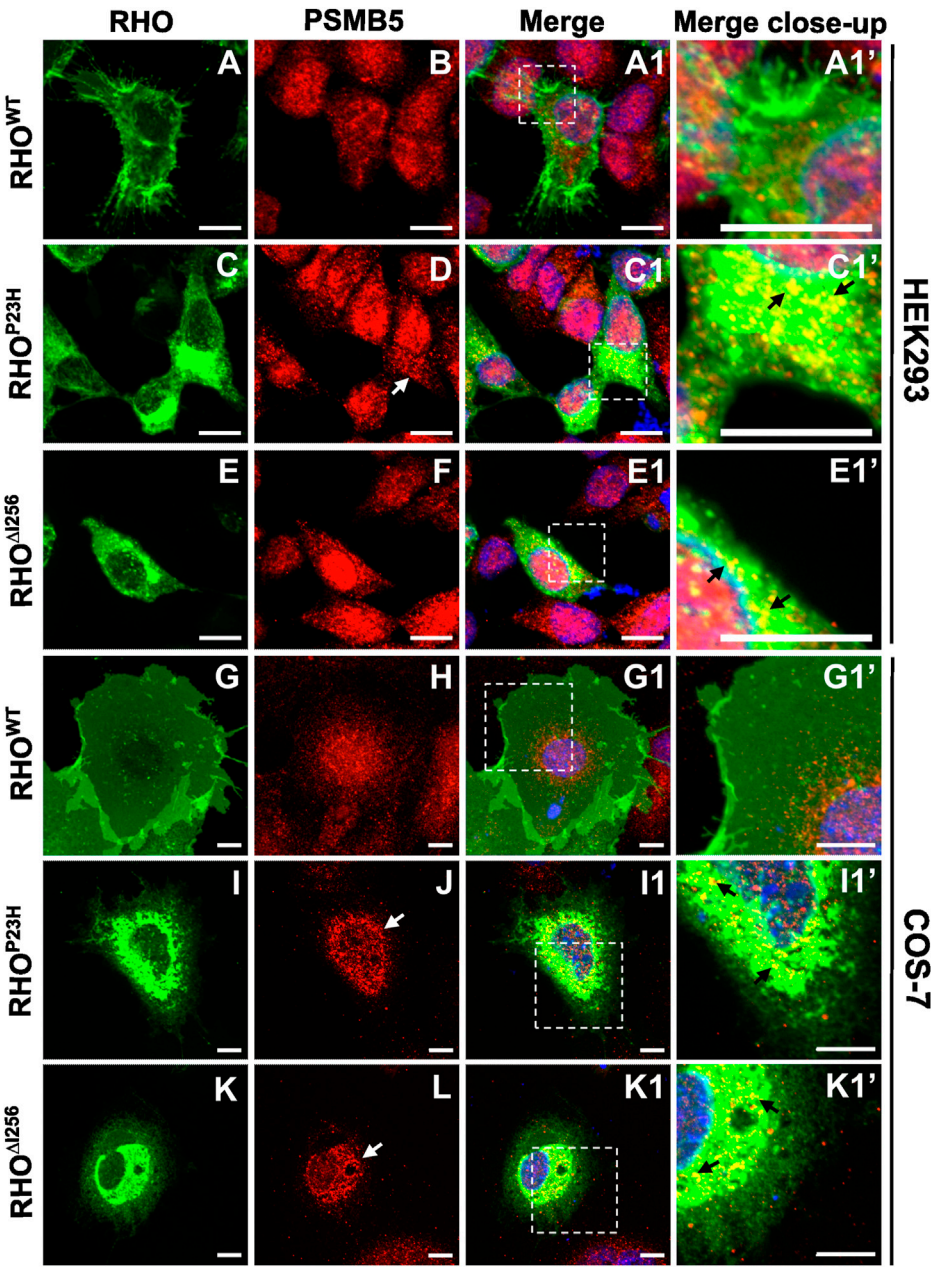

FIGURE 6
Rho$^{\Delta I256}$ is targeted to the proteasome system. Co-staining of EGFP-tagged RHO$^{\Delta I256}$, RHO^{WT}, or RHO^{P23H} (green, first column) with PSMB5 (red, second column) in HEK293 **(A–E1')** and COS-7 cells **(G–K1')**. Colocalization is shown in merged pictures (third column). PSMB5 distributed in the cytosol and nucleus in *Rho*^{WT}-EGFP transfected cells with no overlapping signal. In *Rho*$^{\Delta I256}$-EGFP transfected cells, PSMB5 partially accumulated in the cytosol (white arrows in **F and L**) and colocalized with RHO$^{\Delta I256}$ aggregates (black arrows in **E1' and K1'**). Similar results were also seen in *Rho*^{P23H}-EGFP transfected cells (white arrows in **D and J**; black arrows in **C1', I1'**). Scale bar: 10 μm.

2.7 Inhibition of VCP- and proteasomal activity increase the abundance of high molecular weight RHO aggregates *in vitro*

The colocalization of RHO$^{\Delta I256}$ with different ERAD pathway markers suggested that the ERAD machinery may likely be involved in the clearance of RHO$^{\Delta I256}$ aggregates. To verify this hypothesis further, we inhibited the proteasome or the chaperone VCP.

HEK293 cells overexpressing *Rho*^{WT}-EGFP, *Rho*$^{\Delta I256}$-EGFP, or *Rho*^{P23H}-EGFP were treated with the proteasome inhibitor MG132 (5 μM), the VCP inhibitor ML240 (2 μM) or vehicle (DMSO, 0.1%), for 6 h. Inhibition with MG132 or ML240 significantly increased the levels of HMW aggregates in the lysates of *Rho*$^{\Delta I256}$-EGFP transfected cells (Figure 7A). The average intensity of the bands corresponding to RHO HMW aggregates (molecular weight≥180 kDa), indicated that MG132 or ML240 significantly increased the amount of HMW proteins compared to the vehicle-treated group. These results suggest that both proteasomal and VCP activity are essential for the degradation of RHO$^{\Delta I256}$ during the ERAD process (Figure 7A1).

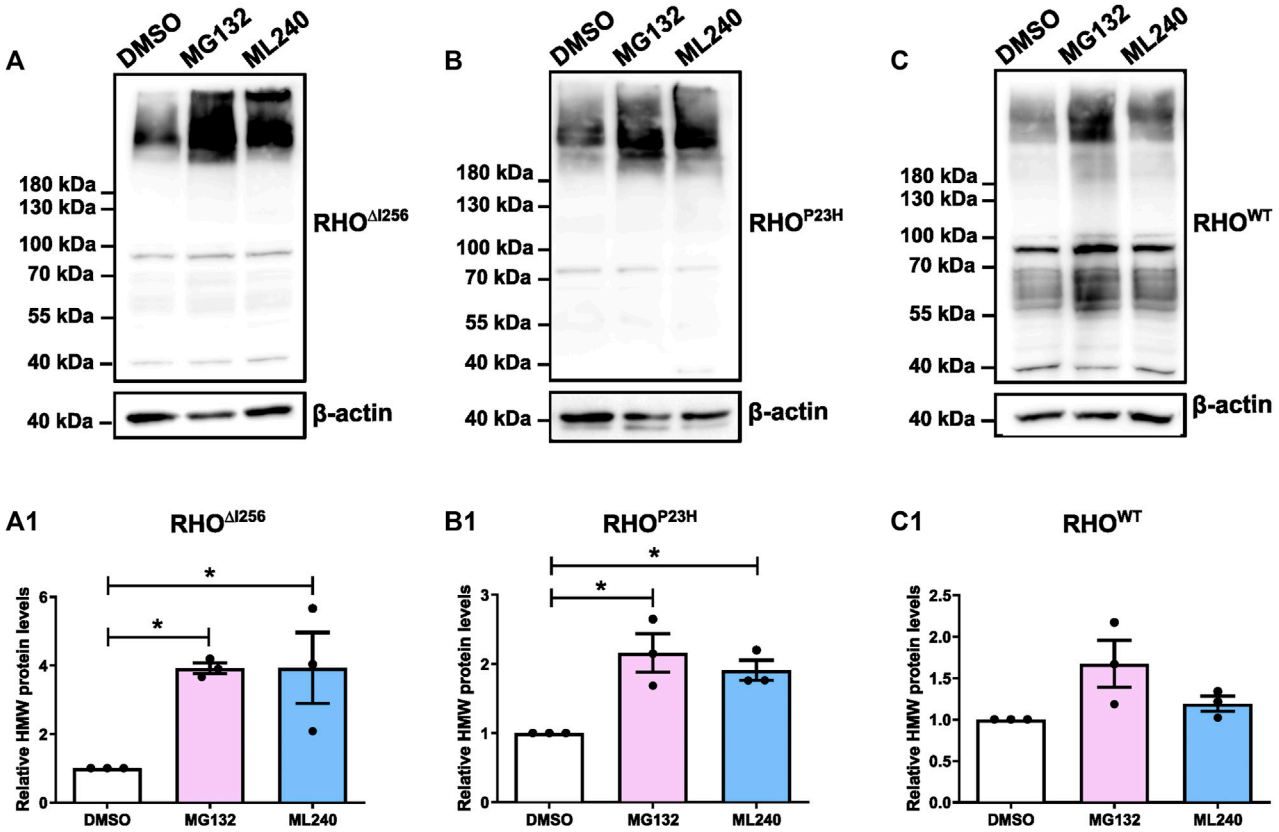

FIGURE 7
Proteasome and VCP inhibition increases HMW aggregates load in *Rho*$^{\Delta I256}$-transfected HEK293 cells. Western blot results for RHO in HEK293 cells after transfection with *Rho*$^{\Delta I256}$-EGFP **(A)**, *Rho*^{P23H}-EGFP **(B)**, or *Rho*^{WT}-EGFP **(C)** followed by treatment with DMSO, 5 μM MG132 or 2 μM ML240 for 6 h. The gray value changes in HMW rhodopsin aggregates bands above 180 kDa following ML132 or ML240 treatment relative to DMSO vehicle treatment is quantified and presented in **(A1, B1, and C1)**. β-actin serves as housekeeping protein control. Data were expressed as mean ± SEM. Significance was calculated by a one-way ANOVA and Bonferroni's multiple comparisons test. *$p < 0.05$. Three independent experiments are included in this data analysis.

The levels of RHO^{P23H} HMW aggregates also significantly increased after MG132 or ML240 treatment, which is consistent with previous findings (Figure 7B, B1) (Illing et al., 2002; Griciuc et al., 2010a; Griciuc et al., 2010b). In addition, the RHO^{WT} HMW aggregates increased slightly, suggesting that RHO^{WT}, when overexpressed, also requires the proteasome for degradation (Figure 7C, C1).

3 Discussion

Rho mutations, a principal cause of adRP, result in changes in protein structure and function. They are classified into seven classes, each with varying defects, including misfolding and disruptions in proteostasis, mislocalization, disrupted intracellular trafficking, instability, and altered function (Athanasiou et al., 2018). The *Rho*$^{\Delta I256}$ mutation is a prevalent primary cause of adRP in a large British kindred as well as in patients from other Western European countries and China (Inglehearn et al., 1991; Artlich et al., 1992; Lorenz et al., 1993b; Li et al., 2010). So far, the precise mechanism and biochemical defects linking it to photoreceptor degeneration have remained unclear.

Our study reveals, for the first time, that a dominant-negative (DN) effect significantly contributes to *Rho*$^{\Delta I256}$-associated retinal degeneration. RHO$^{\Delta I256}$ accumulates in the endoplasmic reticulum (ER) as a substrate for VCP-dependent ER-associated degradation (ERAD). Like RHO^{P23H}, RHO$^{\Delta I256}$ forms perinuclear aggregates, hindering RHO^{WT} from targeting the plasma membrane in cell models or reaching rod outer segments (ROS) in retinal explants. We show here that RHO$^{\Delta I256}$ aggregates colocalize with VCP and undergo polyubiquitination before being retrotranslocated from the ER to the proteasome system. When inhibiting these processes pharmacologically, we observed decreased clearance of aggregates, indicating that both VCP and the proteasome play critical roles in the degradation of RHO$^{\Delta I256}$ aggregates.

Biochemical analysis using HEK293 and COS-7 cells as models demonstrates that, unlike RHO^{WT} and very similar to RHO^{P23H}, RHO$^{\Delta I256}$ protein mislocalizes in the perinuclear region of the cell cytosol, failing to target the cell membrane. Detergent-soluble and detergent-insoluble lysate fractions revealed a higher tendency for RHO$^{\Delta I256}$ than RHO^{WT} to form aggregates, including high molecular weight (HMW) aggregates exceeding 180 kDa, which is in line with previous studies (Sung et al., 1993). This again resembles aggregation patterns seen with RHO^{P23H} (Illing et al., 2002; Griciuc et al., 2010a). Yet, there is a higher tendency for RHO$^{\Delta I256}$ to form HMW aggregates than RHO^{P23H}. This finding goes in line with clinical observations that patients with *Rho*$^{\Delta I256}$

experience a more severe natural history of disease than those with *Rho*^{P23H} (Inglehearn et al., 1991; Artlich et al., 1992; Lorenz et al., 1993a). This could be, at least in part, due to the fact that the deletion of one of the two isoleucine at position 255 or 256 within the sixth transmembrane domain of RHO shortens this intramembrane stretch significantly, affecting the subsequent 20 amino acids as well (Lorenz et al., 1993a).

Given that under normal conditions, RHO likely acts as a functional dimer, the impaired functionality of oligomeric aggregates is expected, hindering normal processes like G protein coupling, interaction with RHO kinase, and engagement with arrestin in the phototransduction cascade (Chabre and Le Maire, 2001; Whorton et al., 2007; Whorton et al., 2008). Nevertheless, the precise mechanisms of how these aggregates lead to cell death remain unknown. A dominant-negative (DN) effect of the mutant protein on the normal protein was reported to account for the dominance of other mutant *Rho* alleles in adRP inheritance (Illing et al., 2002; Saliba PMM et al., 2002; Wilson and Wensel, 2003; Griciuc, 2010). To explore whether RHO$^{\Delta I256}$ has an effect on RHO^{WT}, we conducted an experiment co-expressing EGFP-tagged *Rho*$^{\Delta I256}$ with mcherry-tagged *Rho*^{WT} in cells at equivalent dosage, mirroring conditions observed in *RHO*$^{\Delta I256}$ heterozygous patients. The result revealed significant retention of RHO^{WT} protein in the cell cytosol, colocalizing with intracellular RHO$^{\Delta I256}$ aggregates. Similar outcomes were observed in cells co-transfected with *Rho*^{P23H} and *Rho*^{WT}, aligning with prior studies demonstrating that the *RHO*^{P23H} mutation disrupts *RHO*^{WT} processing, leading to protein inclusions within the cell and impeding RHO^{WT} delivery to the plasma membrane (Illing et al., 2002). In contrast, co-expression of *Rho*^{WT}-EGFP with *Rho*^{WT}-mcherry did not result in aggregates with both RHO^{WT} fusion proteins reaching the cell membrane. These findings confirm the dominant interference of both *Rho*$^{\Delta I256}$ and *Rho*^{P23H} into overall RHO trafficking, suggesting the physical interaction between mutant and wild-type protein.

We extended our study to a three-dimensional retinal explant culture system to better evaluate the DN effect in a more biologically and clinically relevant model. We expressed exogenous *Rho* plasmids in C57BL/6J (WT) retinal explants using the Magnetofection™ method (Sen et al., 2021a; Bassetto et al., 2021). In WT retinae transfected with mutant *Rho*$^{\Delta I256}$-EGFP or *Rho*^{P23H}-EGFP plasmids, fluorescence emitted by *Rho*$^{\Delta I256}$-EGFP overlapped with that of RHO^{WT} protein in the ONL, contrasting with *Rho*^{WT}-EGFP-transfected retinae where both endogenous as well as exogenous RHO^{WT} accurately localized to the OS. These results demonstrate that mutant RHO influences the expression or trafficking of endogenous RHO^{WT}, confirming the DN effect of *Rho*$^{\Delta I256}$ as well as that of *Rho*^{P23H} in -adRP. Our findings on *Rho*^{P23H} align with studies showing the interaction between RHO^{P23H} aggregates and RHO^{WT} through Förster resonance energy transfer (FRET) (Rajan and Kopito, 2005). Other publications affirm that while RHO^{P23H} does aggregate; however, there is no physical interaction with RHO^{WT} (Gragg and Park, 2018). Nonetheless, all studies, including ours, report colocalization between RHO^{P23H} and RHO^{WT} under microscopy, consistent with the notion that these different mutant RHOs hinder the correct trafficking of RHO^{WT} to the plasma membrane. ER retention of aberrant RHO aggregates is one typical feature of class II adRP (Athanasiou et al., 2018). *Rho*$^{\Delta I256}$ falls into this category, and we suggest it belongs to class II.

We found *Rho*$^{\Delta I256}$ to form ER-associated aggregates colocalizing with VCP, ubiquitin, and the proteasome system, three important components of the ERAD process. RHO^{WT} experiences repeated cycles of internalization-degradation (Satoh and Ready, 2005), and in our current study, RHO^{WT} accumulated after VCP and proteasome inhibition, suggesting that RHO^{WT} can also undergo ERAD degradation.

In conclusion, our research provides novel evidence supporting a dominant-negative role of the mutant allele in *Rho*$^{\Delta I256}$-mediated retinitis pigmentosa. The observed formation and degradation of RHO$^{\Delta I256}$ aggregates through the VCP-dependent ERAD pathway makes it a candidate for pharmacological therapy through VCP inhibition. The whole process was described in graphical abstract (Figure 8).

However, further validation in animal model systems is crucial to confirm both the classification of *Rho*$^{\Delta I256}$ as a class II adRP and a possible therapeutic option of targeting the VCP-dependent ERAD pathway for this form of adRP.

4 Materials and methods

4.1 Primers design, cloning, and *E. coli* transformation

Plasmids pEGFP-N1 encoding bovine *Rho (WT or P23H)* driven by the CMV promoter were provided by M. Cheetham (Saliba PMM et al., 2002). For the *Rho*$^{\Delta I256}$ mutation, we designed the primers (IDT primer quest tool), forward primer: 5'-CCG CAT GGT CAT CAT GGT CAT CG-3' and reverse primer: 5'-CAG GAA AGC GAT GAC CAT GAT GAC CAT GC-3'. *Rho*$^{\Delta I256}$ was obtained and amplified by PCR using bovine *Rho*^{WT} as template. To harvest single colonies that contained *Rho*$^{\Delta I256}$, chemical transformation of competent *E. coli* was performed with 2.5 μL of PCR reaction product added into 50 μL of cells. After that, plasmid DNA was prepared from small-scale (1.5 mL, miniprep) bacteria cultures using QIAprep Spin Plasmid Miniprep Kit or from large-scale (50 mL) overnight cultures using the PureYield Plasmid Midiprep System. (*Notes: Isoleucine residues at codons 255 and 256 are conserved in bovine and human Rho. So, we designed the deletion of isoleucine at codon 256 based on the wild-type bovine Rho backbone in the pEGFP vector and applied it in our study.*)

4.2 Cell culture and transfections

HEK293 human embryonic kidney cells (CRL-1573, ATCC—Global Bioresource Center) and COS-7 African green monkey kidney fibroblast-like cells (CRL-1651, ATCC—Global Bioresource Center) were cultured in DMEM supplemented with 10% heat-inactivated fetal bovine serum and 1% penicillin/streptomycin (Thermofisher Scientific). In addition, cells were transiently transfected with 1 μg of *Rho* expression plasmids using TransIT-LT1 transfection reagent (MIR2300, Mirus). HEK293 and COS-7 cells were cultured on the Poly-D-lysine (P6407, Sigma) coating 24 well plates with autoclaved glass coverslips (1.2 cm diameter) for immunostaining or 6 well plates without coverslips for Western blot. Cells were transiently transfected with *Rho-EGFP* constructs or co-transfected with *Rho-EGFP* and *Rho*^{WT}*-mcherry* after 80% of cell confluency and incubated for 48 h.

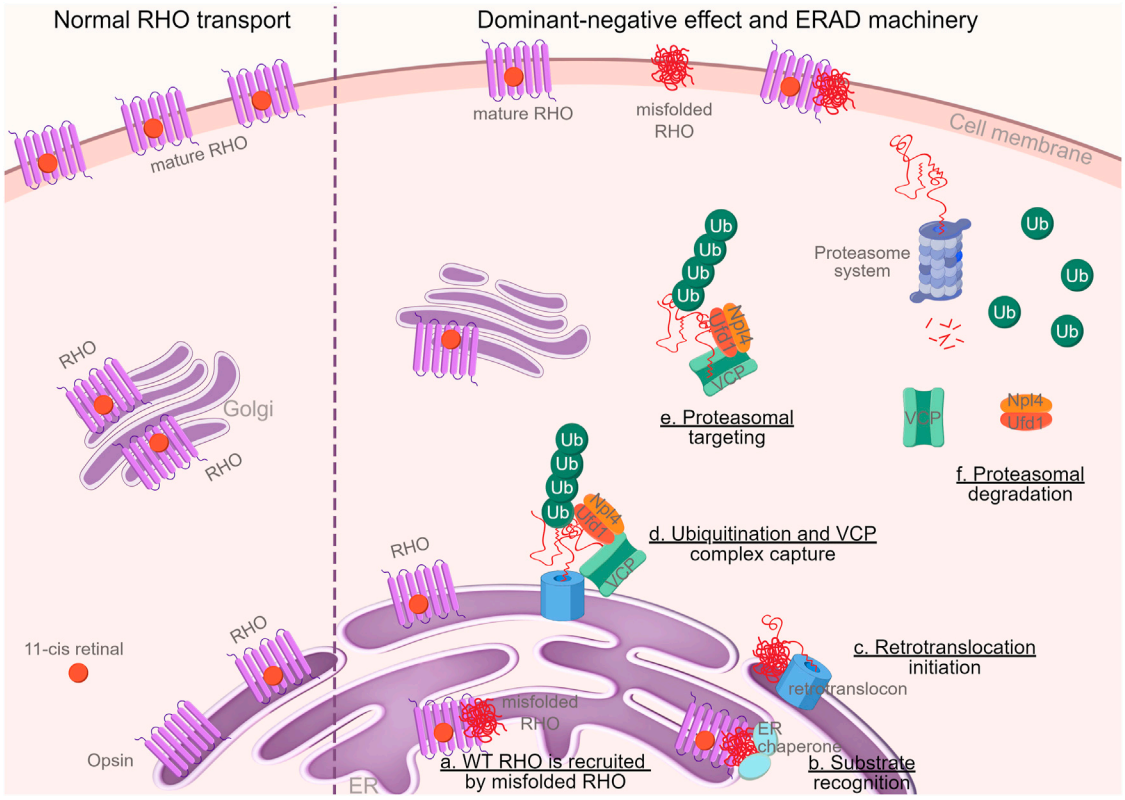

FIGURE 8
Graphical abstract. Schematic illustration of the dominant-negative mechanism of RHO$^{\Delta I256}$ on RHO^{WT} and the degradation of these mutant proteins in the ERAD machinery (*By FigDraw, ID: TWOIA64640*). Misfolded RHO gets withheld in the ER and traps RHO^{WT} (a). Molecular chaperones, such as calnexin, calreticulin, and HSP70, identify misfolded proteins (b) and transport them to the ER retrotranslocation site, where the polypeptides are partially removed from the ER (c) and polyubiquitinated (d). Ubiquitination and VCP complex formation attract ubiquitin fusion degradation 1 (UFD1) and nuclear-protein localization 4 (NPL4) proteins to the retrotranslocon, which initiates the exit of the retrotranslocon from ER to cytoplasm (d). The complex retrotranslocates further into the cytoplasm (step d to e), where VCP-ATPase activity unfolds the protein (e). The unfolded VCP substrate is delivered to the proteasome for full degradation (f) (Vembar and Brodsky, 2008). Ubiquitin, VCP, and other cytosolic chaperones are then recycled.

4.3 Animals

C57BL/6J mice were obtained from Jackson Laboratory (JAX stock #000664, RRID: IMSR_JAX:000664) and housed in the animal facility of the Tübingen Institute for Ophthalmic Research under standard white cyclic lighting, had free access to food and water, and were used irrespective of gender. All procedures were performed in accordance with the Association for Research in Vision and Ophthalmology (ARVO) declaration for the use of animals in ophthalmic and vision research and the law on animal protection issued by the German Federal Government (Tierschutzgesetz) and were approved by the institutional animal welfare office of the University of Tübingen. All efforts were made to minimize the number of animals used and their suffering.

4.4 Immunofluorescence and microscopy

Cells were fixed and stained 48 h after transfection, as described before (Mendes and Cheetham, 2008). Samples were incubated overnight at 4°C with the primary antibodies (calnexin: C5C9, Rabbit monoclonal, 1:100, Cell signaling; VCP: mouse monoclonal, 1:200, Invitrogen; ubiquitin: sc8017, mouse monoclonal, 1:50, Santa Cruz; or proteasome subunit 20S: PSMB5, rabbit polyclonal, 1:100, Invitrogen followed by incubation with secondary antibodies (IgG Alexa Fluor™ 568 or 660 dye-conjugated goat anti-mouse or anti-rabbit respectively, Molecular Probes, Inc. Eugene, United States of America). Negative controls were carried out by omitting the primary antibody. To measure RHO immunofluorescence intensity, the whole cell body of HEK293 cells ($n \geq 40$) and COS-7 cells ($n \geq 20$) of three seperate experimental replicates were carefully contoured, and the fluorescence intensity value was automatically measured by ZEN software. Colocalization analysis using Pearson's correlation coefficient between RHO and ERAD markers was performed using ZEN software. We select at least 6 distinct regions on the cell coverslip for data analysis. All images were captured and analyzed using a Zeiss Axio Imager Z1 ApoTome microscope, AxioCam MRm camera, and Zeiss Zen 2.3 software at 20X or ×63 magnification.

4.5 VCP- and proteasome inhibition assay

HEK293 cells were incubated with 5 μM proteasome inhibitor MG132 (J63250, Alfa Ascar, Thermo Fischer Scientific) or 2 μM VCP inhibitor, ML240 (5,153, Tocris) dissolved in 0.1% DMSO for 6 h after 48 h of transfection. For each inhibitor, 0.1% DMSO was

applied as vehicle control. Cell lysates were then harvested and analyzed by Western blot.

4.6 Western blot

HEK293 cells transfected with *Rho-EGFP* were harvested after 48 h of incubation and then lysed at 4°C in 0.5% Nonident P40 (NP40, Roche) lysis buffer with 1% phosphatase inhibitor cocktail 2 and 3 (PI2 and PI3, Sigma), 2% protease inhibitor complex (PIC, Roche) in TBS. Lysates were centrifuged at 16,000 *g* for 15 min at 4°C. For detergent-insoluble fractions, pellets were solubilized in 1% SDS in PBS at RT, and lysis buffer was added. The pellets were then sonicated at 4°C, and the fraction mixtures were incubated 30 min and then centrifuged at 100 *g* for 10 min, both at 4°C (Griciuc et al., 2010b). For detergent-soluble/-insoluble samples, protein concentration was determined by Bradford assay kits. Cell lysates were normalized for total protein, and 7.5 μg (RHO protein in detergent-soluble), 10 μg (RHO in detergent-insoluble fractions), or 20 μg (Ub protein or RHO protein after VCP inhibition) total protein was prepared and mixed with 1x Laemmli sample buffer before being separated by 8%–16% Tris-Glycine precast gels (Invitrogen) and electroblotted onto PVDF membranes. Immunoblotting was performed according to standard protocols using the as primary antibodies: anti-RHO (1D4, MAB5316, 1:300, Sigma), anti-VCP (MA3-004 1:1,000, Invitrogen), anti-ubiquitin (sc8017, 1:500, Santa Cruz), and anti-β-actin (3700S 1:2000, cell signaling). Afterward, horseradish peroxidase-coupled (HRP) secondary antibodies were applied (1:2000, cell signaling). The ECL Plus chemiluminescent and chemifluorescent HRP detection reagent (Thermo Scientific™ Pierce™ ECL) was used according to the manufacturer's instructions. Band intensity was quantified by *ImageJ* software, and relative protein expression levels were determined based on the WT or untreated control group.

4.7 Organotypic culture preparation and classic magnetofection

In vitro retina cultures were prepared according to published protocols (Arango-Gonzalez et al., 2010). PN9 animals were sacrificed, and the eyeballs were removed and collected in a serum-free R16 culture medium (07490743A, Invitrogen Life Technologies). The eyes were pretreated with 0.12% Proteinase K (0219350490, MP Biomedicals) for 15 min at 37°C in R16 medium. After enzymatic digestion of the eyeball, the retina and the attached pigment epithelium were dissected, and four radial cuts were made to flatten it. Retinas were placed on culture plate inserts (CLS3412, Corning Life Sciences) with the ganglion cell layer uppermost. The retinal explants were cultured in 1 mL serum-free culture medium consisting of Neurobasal A (21103049, Thermo Fischer Scientific) supplemented with 2% B-27 supplement (17504044, Thermo Fischer Scientific), 1% N2 supplement (17502048, Thermo Fischer Scientific), 1% penicillin solution (15140-122, Thermo Fischer Scientific), and 0.4% GlutaMax (35050061, Thermo Fischer Scientific) and maintained at 37°C in a humidified atmosphere with 5% CO_2. At the same time, 2 μg EGFP-tagged Rho^{WT}, Rho^{P23H}, $Rho^{\Delta I256}$ plasmids, and 1.5 μL magnetic nanoparticles (XPMag Explant Transfection Reagent, OZBiosciences) were complexed for 30 min in Neurobasal-A medium, to a total volume of 10 μL. The solution was incubated at room temperature for 30 min to allow the cationic magnetic nanoparticles to bind to the negatively charged DNA plasmids. After complexation, the magnetic complexes were administered to the top of each retina (on the ganglion layer side). The super-magnetic plate was immediately placed under the 6-well plate. Then, the set well plate/magnet was kept in the incubator for 1 h, to allow the pull down of the complexes through the retinae. After removal of the magnet, retinae in the 6-well plates remained incubated at 37°C in 5% CO_2 for 3 days before fixation in 4% paraformaldehyde.

4.8 Preparation and immunohistochemistry on retinal sections

The explants were immersed in 4% paraformaldehyde in 0.1 M phosphate buffer (PB; pH 7.4) for 45 min at RT, followed by cryoprotection in graded sucrose solutions (10%, 20%, 30%) and embedded in cryomatrix (Tissue-Tek® OCT Compound, VWR). Radial sections (14 μm) were collected, air-dried, and stored at −20°C. Retina sections were incubated overnight at 4°C with rhodopsin primary antibody (1D4, MAB5316, 1:300, Sigma) followed by incubation with secondary antibody (Alexa Fluor™ 568 dye-conjugated goat anti-mouse IgG). DAPI (D9542, Sigma) was used as a nuclear counterstain. Finally, the slides were mounted with Fluoromount-G Mounting Medium (17984-25, EMS).

4.9 Statistical analyses

Mann-Whitney-U-test analysis was used to examine RHO MFI that did not match Gaussian distribution; while, Pearson's correlation coefficient and protein gray levels that were consistent with normal distribution were analyzed using one-way ANOVA followed by Bonferroni's *post hoc* comparisons tests in *GraphPad Prism 9* software. Data were presented as mean ± standard error of the mean (SEM). Differences were considered significant and indicated as $^{*}p < 0.05$, $^{**}p < 0.01$, $^{***}p < 0.001$, $^{****}p < 0.0001$.

Data availability statement

The original contributions presented in the study are included in the article/Supplementary Material, further inquiries can be directed to the corresponding authors.

Ethics statement

Ethical approval was not required for the studies on humans in accordance with the local legislation and institutional requirements because only commercially available established cell lines were used. The animal study was approved by all procedures were performed in accordance with the Association for Research in Vision and Ophthalmology (ARVO) declaration for the use of animals in ophthalmic and vision research and the

law on animal protection issued by the German Federal Government (Tierschutzgesetz) and were approved by the institutional animal welfare office of the University of Tübingen. The study was conducted in accordance with the local legislation and institutional requirements.

Author contributions

BC: Conceptualization, Writing–original draft, Visualization, Methodology, Investigation, Formal Analysis, Data curation. JD: Methodology, Writing–review and editing, Investigation, Data curation. MS: Methodology, Writing–review and editing, Investigation. TB: Conceptualization, Writing–review and editing, Methodology. TL: Writing–review and editing, Methodology. EK: Writing–review and editing, Project administration, Writing–original draft, Conceptualization. BA-G: Writing–review and editing, Visualization, Investigation, Formal Analysis, Writing–original draft, Supervision, Project administration, Funding acquisition, Conceptualization. MU: Writing–review and editing, Resources, Investigation, Formal Analysis, Writing–original draft, Supervision, Project administration, Funding acquisition, Conceptualization.

Funding

The author(s) declare that financial support was received for the research, authorship, and/or publication of this article. This work was supported by the Tistou and Charlotte Kerstan Foundation (to MU and BA-G), Fighting Blindness Canada (FBC)—2022–23 Transformative Research Award (to MU and BA-G) and by institutional funds to MU.

Acknowledgments

The animal husbandry personnel at the Universitätsklinikum Tübingen and Norman Rieger are acknowledged for providing animal care. We acknowledge support from the Open Access Publishing Fund of the University of Tübingen, and gratefully acknowledge the support from the China Scholarship Council (grant number 201808080183).

Conflict of interest

The authors declare that the research was conducted in the absence of any commercial or financial relationships that could be construed as a potential conflict of interest.

Publisher's note

All claims expressed in this article are solely those of the authors and do not necessarily represent those of their affiliated organizations, or those of the publisher, the editors and the reviewers. Any product that may be evaluated in this article, or claim that may be made by its manufacturer, is not guaranteed or endorsed by the publisher.

Supplementary material

The Supplementary Material for this article can be found online at: https://www.frontiersin.org/articles/10.3389/fmolb.2024.1369000/full#supplementary-material

References

Adams, J. (2003). The proteasome: structure, function, and role in the cell. *Cancer Treat. Rev.* 29 (1), 3–9. doi:10.1016/s0305-7372(03)00081-1

Arango-Gonzalez, B., Sen, M., Guarascio, R., Ziaka, K., del Amo, E. M., Hau, K., et al. (2020) *Inhibition of VCP preserves retinal structure and function in autosomal dominant retinal degeneration*. Biorxiv.

Arango-Gonzalez, B., Szabo, A., Pinzon-Duarte, G., Lukats, A., Guenther, E., and Kohler, K. (2010). *In vivo* and *in vitro* development of S- and M-cones in rat retina. *Invest. Ophthalmol. Vis. Sci.* 51 (10), 5320–5327. doi:10.1167/iovs.09-4741

Artlich, A., Horn, M., Lorenz, B., Bhattacharga, S., and Gal, A. (1992). Recurrent 3-bp deletion at codon 255/256 of the rhodopsin gene in a German pedigree with autosomal dominant retinitis pigmentosa. *Am. J. Hum. Genet.* 50 (4), 876–878.

Athanasiou, D., Aguila, M., Bellingham, J., Li, W., McCulley, C., Reeves, P. J., et al. (2018). The molecular and cellular basis of rhodopsin retinitis pigmentosa reveals potential strategies for therapy. *Prog. Retin Eye Res.* 62, 1–23. doi:10.1016/j.preteyeres.2017.10.002

Bassetto, M., Sen, M., Poulhes, F., Arango-Gonzalez, B., Bonvin, E., Sapet, C., et al. (2021). New method for efficient siRNA delivery in retina explants: reverse magnetofection. *Bioconjug Chem.* 32 (6), 1078–1093. doi:10.1021/acs.bioconjchem.1c00132

Bence, N. F., Sampat, R. M., and Kopito, R. R. (2001). Impairment of the ubiquitin-proteasome system by protein aggregation. *Science.* 292 (5521), 1552–1555. doi:10.1126/science.292.5521.1552

Berson, E. L. (1996). Retinitis pigmentosa Unfolding its mystery. *Proc. Natl. Acad. Sci.* 93, 4526–4528. doi:10.1073/pnas.93.10.4526

Boeddrich, A., Gaumer, S., Haacke, A., Tzvetkov, N., Albrecht, M., Evert, B. O., et al. (2006). An arginine/lysine-rich motif is crucial for VCP/p97-mediated modulation of ataxin-3 fibrillogenesis. *EMBO J.* 25 (7), 1547–1558. doi:10.1038/sj.emboj.7601043

Chabre, M., and Le Maire, M. (2001). Monomeric G-protein-coupled receptor as a functional unit. *Biochemistry* 44 (27), 9395–9403. doi:10.1021/bi050720o

Cross, N., van Steen, C., Zegaoui, Y., Satherley, A., and Angelillo, L. (2022). Retinitis pigmentosa: burden of disease and current unmet needs. *Clin. Ophthalmol.* 16, 1993–2010. doi:10.2147/OPTH.S365486

Daiger, S. P., Bowne, S. J., and Sullivan, L. S. (2007). Perspective on genes and mutations causing retinitis pigmentosa. *ArchOphthalmol* 125 (2), 151–158. doi:10.1001/archopht.125.2.151

Deretic, D. (2006). A role for rhodopsin in a signal transduction cascade that regulates membrane trafficking and photoreceptor polarity. *Vis. Res.* 46 (27), 4427–4433. doi:10.1016/j.visres.2006.07.028

Downer, N. W., and Cone, R. A. (1985). Transient dichroism in photoreceptor membranes indicates that stable oligomers of rhodopsin do not form during excitation. *Biophysical J.* 47 (3), 277–284. doi:10.1016/S0006-3495(85)83917-5

Dryja, T. P., McGee, T. L., Reichel, E., Hahn, L. B., Cowley, G. S., Yandell, D. W., et al. (1990). A point mutation of the rhodopsin gene in one form of retinitis pigmentosa. *Nature* 343 (6256), 364–366. doi:10.1038/343364a0

Frick, K. D., RoebuckFeldstein, MCJI, McCarty, C. A., and Grover, L. L. (2012). Health services utilization and cost of retinitis pigmentosa. *Arch. Ophthalmol.* 130 (5), 629–634. doi:10.1001/archophthalmol.2011.2820

Gitcho, M. A., Strider, J., Carter, D., Taylor-Reinwald, L., Forman, M. S., Goate, A. M., et al. (2009). VCP mutations causing frontotemporal lobar degeneration disrupt localization of TDP-43 and induce cell death. *J. Biol. Chem.* 284 (18), 12384–12398. doi:10.1074/jbc.M900992200

Gomez-Tourino, I. M., Senra, A., and Garcia, F. (2013). Nucleofection of whole murine retinas. *Cytotechnology* 65 (4), 523–532. doi:10.1007/s10616-012-9509-3

Gragg, M., and Park, P. S. H. (2018). Misfolded rhodopsin mutants display variable aggregation properties. *Biochim. Biophys. Acta Mol. Basis Dis.* 1864 (9), 2938–2948. doi:10.1016/j.bbadis.2018.06.004

Griciuc, A. (2010) *Molecular and functional analysis of the ERAD effector VCP in cellular and Drosophila models for retinitis pigmentosa*. Germany: Technische Universität München.

Griciuc, A., Aron, L., Piccoli, G., and Ueffing, M. (2010a). Clearance of Rhodopsin(P23H) aggregates requires the ERAD effector VCP. *Biochim. Biophys. Acta* 1803 (3), 424–434. doi:10.1016/j.bbamcr.2010.01.008

Griciuc, A., Aron, L., Roux, M. J., Klein, R., Giangrande, A., and Ueffing, M. (2010b). Inactivation of VCP/ter94 suppresses retinal pathology caused by misfolded rhodopsin in Drosophila. *PLoS Genet.* 6 (8), e1001075. doi:10.1371/journal.pgen.1001075

Guerriero, C. J., and Brodsky, J. L. (2012). The delicate balance between secreted protein folding and endoplasmic reticulum-associated degradation in human physiology. *Physiol. Rev.* 92 (2), 537–576. doi:10.1152/physrev.00027.2011

Hargrave, P. A. (2001). Rhodopsin structure, function, and topography the Friedenwald lecture. *Invest. Ophthalmol. Vis. Sci.* 42 (1), 3–9.

Hartong, D. T., Berson, E. L., and Dryja, T. P. (2006). Retinitis pigmentosa. *Lancet.* 368 (9549), 1795–1809. doi:10.1016/S0140-6736(06)69740-7

Herskowitz, I. (1987). Functional inactivation of genes by dominant negative mutations. *Nature* 329, 219–222. doi:10.1038/329219a0

Humphries, M. M., Rancourt, D., Farrar, G. J., Kenna, P., Hazel, M., Bush, R. A., et al. (1997). Retinopathy induced in mice by targeted disruption of the rhodopsin gene. *Nat. Genet.* 15, 216–219. doi:10.1038/ng0297-216

Illing, M. E., Rajan, R. S., Bence, N. F., and Kopito, R. R. (2002). A rhodopsin mutant linked to autosomal dominant retinitis pigmentosa is prone to aggregate and interacts with the ubiquitin proteasome system. *J. Biol. Chem.* 277 (37), 34150–34160. doi:10.1074/jbc.M204955200

Inglehearn, C. F., Bashir, R., Lester, D. H., Jay, M., Bird, A. C., and Bhattacharya, S. S. (1991). A 3-bp deletion in the rhodopsin gene in a family with autosomal dominant retinitis pigmentosa. *Am. J. Hum. Genet.* 48 (1), 26–30.

Kaushal, S., and Khorana, H. G. (1994). Structure and function in rhodopsin. 7. Point mutations associated with autosomal dominant retinitis pigmentosa. *Biochemistry* 33 (20), 6121–6128. doi:10.1021/bi00186a011

Krebs, M. P., Holden, D. C., Joshi, P., Clark, C. L., 3rd, Lee, A. H., and Kaushal, S. (2010). Molecular mechanisms of rhodopsin retinitis pigmentosa and the efficacy of pharmacological rescue. *J. Mol. Biol.* 395 (5), 1063–1078. doi:10.1016/j.jmb.2009.11.015

Lem, J., Krasnopernova, N. V., Calvert, P. D., Kosaras, B., Cameron, D. A., Nicolo, M., et al. (1999). Morphological, physiological, and biochemical changes in rhodopsin knockout mice. *Proc. Natl. Acad. Sci.* 96, 736–741. doi:10.1073/pnas.96.2.736

Li, S., Xiao, X., Wang, P., Guo, X., and Zhang, Q. (2010). Mutation spectrum and frequency of the RHO gene in 248 Chinese families with retinitis pigmentosa. *Biochem. Biophys. Res. Commun.* 401 (1), 42–47. doi:10.1016/j.bbrc.2010.09.004

Lorenz, B., Hormann, C., Horn, M., Berninger, B., Döring, M., and Gal, A. (1993b) *Ocular findings in patients with autosomal dominant retinitis pigmentosa due to a 3-base pair deletion at codon 255/256 of the human rhodopsin gene. Retinal degeneration*. Berlin, Germany: Springer Nature, 103–114.

Lorenz, B., Hörmann, C., Horn, M., Berninger, T., Döring, M., and Gal, A. (1993a). "Ocular findings in patients with autosomal dominant retinitis pigmentosa due to a 3-base pair deletion at codon 255/256 of the human rhodopsin gene," in *Retinal degeneration: clinical and laboratory applications*. Editors J. G. Hollyfield, R. E. Anderson, and M. M. LaVail (Boston, MA: Springer US), 103–114.

Mendes, H. F., and Cheetham, M. E. (2008). Pharmacological manipulation of gain-of-function and dominant-negative mechanisms in rhodopsin retinitis pigmentosa. *Hum. Mol. Genet.* 17 (19), 3043–3054. doi:10.1093/hmg/ddn202

Mendes, H. F., van der, S. J., Chapple, J. P., and Cheetham, M. E. (2005). Mechanisms of cell death in rhodopsin retinitis pigmentosa: implications for therapy. *Trends MolMed* 11 (4), 177–185. doi:10.1016/j.molmed.2005.02.007

Milam, A. H., Li, Z. Y., Cideciyan, A. V., and Jacobson, S. G. (1996). Clinicopathologic effects of the Q64ter rhodopsin mutation in retinitis pigmentosa. *Invest. Ophthalmol. Vis. Sci.* 37 (5), 753–765.

Mizuno, Y., Hori, S., Kakizuka, A., and Okamoto, K. (2003). Vacuole-creating protein in neurodegenerative diseases in humans. *Neurosci. Lett.* 343 (2), 77–80. doi:10.1016/s0304-3940(03)00280-5

Naash, M. I., Hollyfield, J. G., Al-Ubaidi, M. R., and Baehr, W. (1993). Simulation of human autosomal dominant retinitis pigmentosa in transgenic mice expressing a mutated murine opsin gene. *ProcNatlAcadSciUSA* 90 (12), 5499–5503. doi:10.1073/pnas.90.12.5499

Pearring, J. N., Salinas, R. Y., Baker, S. A., and Arshavsky, V. Y. (2013). Protein sorting, targeting and trafficking in photoreceptor cells. *Prog. Retin Eye Res.* 36, 24–51. doi:10.1016/j.preteyeres.2013.03.002

Rajan, R. S., and Kopito, R. R. (2005). Suppression of wild-type rhodopsin maturation by mutants linked to autosomal dominant retinitis pigmentosa. *J. Biol. Chem.* 280 (2), 1284–1291. doi:10.1074/jbc.M406448200

Rakoczy, E. P., Kiel, C., McKeone, R., Stricher, F., and Serrano, L. (2011). Analysis of disease-linked rhodopsin mutations based on structure, function, and protein stability calculations. *J. Mol. Biol.* 405 (2), 584–606. doi:10.1016/j.jmb.2010.11.003

Rakshit, T., and Park, P. S. (2015). Impact of reduced rhodopsin expression on the structure of rod outer segment disc membranes. *Biochemistry* 54 (18), 2885–2894. doi:10.1021/acs.biochem.5b00003

Sakai, T., Calderone, J. B., Lewis, G. P., Linberg, K. A., Fisher, S. K., and Jacobs, G. H. (2003). Cone photoreceptor recovery after experimental detachment and reattachment: an immunocytochemical, morphological, and electrophysiological study. *Invest. Ophthalmol. Vis. Sci.* 44 (1), 416–425. doi:10.1167/iovs.02-0633

Saliba Pmm, R. S., Luthert, P. J., and Cheetham, M. E. (2002). The cellular fate of mutant rhodopsin: quality control, degradation and aggresome formation. *J. Cell Sci.* 115 (14), 2907–2918. doi:10.1242/jcs.115.14.2907

Satoh, A. K., and Ready, D. F. (2005). Arrestin1 mediates light-dependent rhodopsin endocytosis and cell survival. *Curr. Biol.* 15 (19), 1722–1733. doi:10.1016/j.cub.2005.08.064

Schwartz, A. L., and Ciechanover, A. (2009). Targeting proteins for destruction by the ubiquitin system: implications for human pathobiology. *Annu. Rev. Pharmacol. Toxicol.* 49, 73–96. doi:10.1146/annurev.pharmtox.051208.165340

Sen, M., Bassetto, M., Poulhes, F., Zelphati, O., Ueffing, M., and Arango-Gonzalez, B. (2021a). Efficient ocular delivery of VCP siRNA via reverse magnetofection in RHO P23H rodent retina explants. *Pharmaceutics* 13 (2), 225. doi:10.3390/pharmaceutics13020225

Sen, M., Kutsyr, O., Cao, B., Bolz, S., Arango-Gonzalez, B., and Ueffing, M. (2021b). Pharmacological inhibition of the VCP/proteasome Axis rescues photoreceptor degeneration in RHO(P23H) rat retinal explants. *Biomolecules* 11 (10), 1528. doi:10.3390/biom11101528

Sullivan, L. S., Bowne, S. J., Birch, D. G., Hughbanks-Wheaton, D., Heckenlively, J. R., Lewis, R. A., et al. (2006). Prevalence of disease-causing mutations in families with autosomal dominant retinitis pigmentosa: a screen of known genes in 200 families. *Invest. Ophthalmol. Vis. Sci.* 47 (7), 3052–3064. doi:10.1167/iovs.05-1443

Sung, C. H., Davenport, C. M., and Nathans, J. (1993). Rhodopsin mutations responsible for autosomal dominant retinitis pigmentosa. Clustering of functional classes along the polypeptide chain. *JBiolChem* 268 (35), 26645–26649. doi:10.1016/s0021-9258(19)74360-9

Vembar, S. S., and Brodsky, J. L. (2008). One step at a time: endoplasmic reticulum-associated degradation. *Nat. Rev. Mol. Cell Biol.* 9 (12), 944–957. doi:10.1038/nrm2546

Wang, Q., Song, C., and Li, C. C. (2004). Molecular perspectives on p97-VCP: progress in understanding its structure and diverse biological functions. *J. Struct. Biol.* 146 (1-2), 44–57. doi:10.1016/j.jsb.2003.11.014

Whorton, M. R., Bokoch, M. P., Rasmussen, S. G., Huang, B., Zare, R. N., Kobilka, B., et al. (2007). A monomeric G protein-coupled receptor isolated in a high-density lipoprotein particle efficiently activates its G protein. *Proc. Natl. Acad. Sci. U. S. A.* 104 (18), 7682–7687. doi:10.1073/pnas.0611448104

Whorton, M. R., Jastrzebska, B., Park, P. S., Fotiadis, D., Engel, A., Palczewski, K., et al. (2008). Efficient coupling of transducin to monomeric rhodopsin in a phospholipid bilayer. *J. Biol. Chem.* 283 (7), 4387–4394. doi:10.1074/jbc.M703346200

Wilson, J. H., and Wensel, T. G. (2003). The nature of dominant mutations of rhodopsin and implications for gene therapy. *Mol. Neurobiol.* 28 (2), 149–158. doi:10.1385/MN:28:2:149

Ye, Y., Meyer, H. H., and Rapoport, T. A. (2001). The AAA ATPase Cdc48/p97 and its partners transport proteins from the ER into the cytosol. *Nature* 414 (6864), 652–656. doi:10.1038/414652a